# Specification of positional identity in forebrain organoids

**Gustav Y. Cederquist[1,2], James J. Asciolla[3,4], Jason Tchieu[1], Ryan M. Walsh[1], Daniela Cornacchia [1], Marilyn D. Resh[3,4] and Lorenz Studer [1]***

**Human brain organoids generated with current technologies recapitulate histological features of the human brain, but they lack a reproducible topographic organization. During development, spatial topography is determined by gradients of signaling molecules released from discrete signaling centers. We hypothesized that introduction of a signaling center into forebrain organoids would specify the positional identity of neural tissue in a distance-dependent manner. Here, we present a system to trigger a Sonic Hedgehog (SHH) protein gradient in developing forebrain organoids that enables ordered self-organization along dorso-ventral and antero-posterior positional axes. SHH-patterned forebrain organoids establish major forebrain subdivisions that are positioned with *in vivo*-like topography. Consistent with its behavior *in vivo*, SHH exhibits long-range signaling activity in organoids. Finally, we use SHH-patterned cerebral organoids as a tool to study the role of cholesterol metabolism in SHH signaling. Together, this work identifies inductive signaling as an effective organizing strategy to recapitulate *in vivo*-like topography in human brain organoids.**

Human pluripotent stem cells (hPSCs) have the intrinsic capacity to self-organize into multicellular organ-like structures called organoids[1,2]. Brain organoids recapitulate the cellular diversity and micro-architectural features characteristic of discrete brain regions, providing unprecedented opportunities to model human brain development and disease[3–5]. However, in these organoids, individual brain regions are ordered randomly and non-reproducibly and lack the characteristic *in vivo* anterior-posterior, dorso-ventral, and medio-lateral positioning that supports the emergence of complex brain structure and function[1,4,6]. The absence of a defined topography is a crucial shortcoming of current brain organoid technologies.

During brain development, topographic maps are generated by gradients of signaling activity that allow cells to acquire discrete regional identities as a function of their position[7,8]. Region-specific organoids attempt to overcome positional heterogeneity by restricting cellular identities to a single brain area, such as the optic cup[9], adenohypophysis[10], forebrain[11], midbrain[12], or hindbrain[13], using bath-application of patterning factors[14]. More recently, several groups have created a dorso-ventral axis by fusing dorsal and ventral forebrain organoids[15–17]. While these strategies recapitulate some processes associated with long-range tissue interactions, such as cell migration, they fail to capture the full continuum of regional diversity encompassed by the human forebrain.

Sonic Hedgehog (SHH) is a signaling factor whose graded expression specifies the spatial organization of discrete progenitor domains across the neuraxis[18,19]. To test whether introduction of a SHH signaling gradient into developing forebrain organoids could specify positional domains, we engineered an inducible SHH-expressing hPSC line (iSHH) that could be embedded at one pole of a developing organoid (Fig. 1a). The iSHH line was generated by TALEN-mediated gene targeting into the *AAVS1* locus of an hPSC line with constitutive RFP expression[20,21]. A constitutively active reverse tetracycline transactivator is expressed from one allele of the *AAVS1* locus, while full-length human *SHH* is expressed from the other allele, under the control of a tetracycline response element (TRE) (Fig. 1a). This strategy resulted in titratable *SHH* expression (Fig. 1b) and commensurate post-translational palmitoylation (Supplementary Fig. 1a). The iSHH line induced robust expression of the SHH target gene *FOXA2* during neural differentiation in the presence of doxycycline, indicating appropriate biological activity (Fig. 1c).

We next developed a method to embed iSHH cells at one pole of an hPSC spheroid, mimicking a developmental organizer. First, 1,000 iSHH cells were seeded in low-attachment round bottom microwells and allowed to aggregate for 24 h (day −2 to −1). The next day 10,000 wild-type H9 hPSC were seeded on top of the iSHH cells (day −1 to 0) and allowed to aggregate for another 24 h, resulting in a reproducible chimeric iSHH-H9 spheroid in which a small cluster of iSHH cells are embedded within a larger spheroid (Supplementary Fig. 1b, >90% efficiency). We refer to these chimeric 3D hPSC cultures as SHH-spheroids. For the specific induction of forebrain identity, we devised a strategy that combines aspects of several previous organoid induction protocols. In brief, SHH-spheroids were cultured in the presence of inhibitors of TGFβ, BMP, and WNT (3-inhibitor protocol) for 6–8 d to promote specification of anterior forebrain identity[11]. After 6–8 d of differentiation, spheroids were embedded in matrigel droplets to promote neuroepithelial organization and moved to an orbital shaker upon outgrowth of neuroepithelial buds, which was typically 4–6 d[4] (Supplementary Fig. 1c). Doxycycline (400 ng/ml) was added to the differentiation medium starting at day 0 to induce an asymmetric SHH signal (Fig. 1d). Under those conditions, the iSHH-organizer typically remained positioned at one end of the developing organoid, though we observed small clusters of organizer cells separated from the main organizer in 25% of instances (Supplementary Fig. 1d). To assess whether this strategy generates a gradient of SHH protein, we performed immunocytochemistry at day 4 of the differentiation. In the absence of doxycycline, no SHH protein was detectable.

[1]The Center for Stem Cell Biology, Developmental Biology Program, Sloan-Kettering Institute for Cancer Research, New York, NY, USA. [2]Weill-Cornell/Rockefeller/Sloan-Kettering Tri-Institutional MD-PhD Program, New York, NY, USA. [3]Cell Biology Program, Memorial Sloan-Kettering Cancer Center, New York, NY, USA. [4]Biochemistry, Cell Biology and Molecular Biology Graduate Program, Weill Cornell Graduate School of Medical Sciences, New York, NY, USA. *e-mail: studerl@mskcc.org

In the presence of doxycycline, high levels of SHH expression were detected in the region of the iSHH cells, and the abundance of SHH protein was reduced as a function of distance from the SHH-organizer (Fig. 1e,f).

Functional subdivisions in the mammalian forebrain are located at discrete positions within a Cartesian coordinate system, whose axes are arranged in the dorso-ventral, medio-lateral, and antero-posterior directions. Each of the dorso-ventral and antero-posterior domains can be identified by the expression of characteristic transcription factors. PAX6 is expressed in the dorsal forebrain and NKX2.1 in the ventral forebrain (Fig. 1g). FOXG1 is expressed in the anterior forebrain, or telencephalon, while it is absent from the posterior forebrain, or diencephalon. In contrast, OTX2 is expressed in the diencephalon (Fig. 1h). When we differentiated H9 spheroids or SHH-spheroids in the absence of doxycycline, they predominantly expressed PAX6 and FOXG1 within self-organized neuroepithelium, in agreement with previous findings[11] (Fig. 1g,h). This indicates that the default identity of our 3D cultures is dorsal-anterior forebrain, which gives rise to the neocortex. SHH-spheroids grown in the presence of doxycycline (400 ng/ml) induced NKX2.1 near the organizer, while PAX6 expression was suppressed (Fig. 1g).

Surprisingly, FOXG1 expression was also suppressed near the organizer, while OTX2 expression was maintained (Fig. 1h), suggesting that SHH can lead to posterior forebrain specification. We therefore examined the expression of TCF7L2, which is expressed in the diencephalon[22,23] and SIX3[24], which is expressed in optic recess and hypothalamus, in SHH-organoids. Both TCF7L2 and SIX3 were induced near organizer tissue (Fig. 1i), supporting a role for SHH in anterior-posterior patterning, as well as dorsoventral patterning. SHH exhibited dose-dependent induction of *DKK1* (Fig. 1j), a secreted antagonist that shapes the anterior-posterior WNT gradient *in vivo*, that is commonly induced in regions of high WNT/β-catenin activity and that is a critical regulator of anterior-posterior patterning[25–27]. Thus, SHH might exert anterior-posterior patterning activity via regulation of WNT signaling[28].

Given that a SHH protein gradient could specify distinct dorso-ventral and antero-posterior positional domains, we next sought to determine whether the resulting forebrain subdivisions were aligned according to an anatomically appropriate topography. The position of the presumptive forebrain subdivisions *in vivo* can be defined by their distance from the SHH source in the hypothalamus. The neocortex (PAX6+/FOXG1+) represents the anterior and dorsal subdivision of the forebrain, which is located most distal from the SHH source. Just ventral to the neocortex is the lateral ganglionic eminence (LGE), characterized by the co-expression of GSH2 and FOXG1, followed by the medial ganglionic eminence (MGE), characterized by co-expression of NKX2.1 and FOXG1, the antero-dorsal hypothalamus, characterized by expression of NKX2.2, and finally the ventro-posterior hypothalamus, characterized by the expression of NKX2.1 and absence of FOXG1, representing the brain region located most ventral and proximal to the SHH source (Fig. 2a).

When differentiated in the presence of doxycycline (400 ng/ml), SHH-spheroids formed at least five topographically distinct presumptive forebrain domains. Quantification of the distance of forebrain domains from the SHH-organizer (Supplementary Fig. 2), identified by protein expression, revealed that the positioning of these domains mimics the pattern observed *in vivo* (Fig. 2b). Topographic organization could be triggered in a similar manner in at least five additional hPSC or iPSC lines using the same H9-based iSHH organizer, though the specific growth rates and size of regional domains could differ (Supplementary Fig. 3). We next identified presumptive neocortical (FOXG1+/PAX6+), LGE (GSH2+), MGE (FOXG1+/NKX2.1+), anterior hypothalamic (NKX2.2+) and ventro-posterior hypothalamic (NKX2.1+/FOXG1−) regions by immunocytochemistry (Fig. 2c). FOXG1 expression was absent from the organizer tissue itself, but robust expression of NKX2.1 was observed in at least a subset of the organizer cells, suggesting hypothalamic identity[29] (Supplementary Fig. 4a). The resulting topographic patterning is in contrast to the patterning exerted by bath application of SHH agonist to forebrain organoids, which results in

**Fig. 1 | Establishment of dorso-ventral and antero-posterior developmental axes in SHH-organoids. a**, Strategy to specify positional identity in forebrain organoids. SHH exhibits a ventral-high to dorsal-low gradient in the developing forebrain. A doxycycline-inducible SHH (iSHH) hPSC line was engineered using TALEN-mediated homologous recombination. The iSHH line could be positioned at one pole of developing forebrain organoids. **b**, qRT-PCR analysis shows robust and titratable induction of *SHH* transcript expression in iSHH but not H9 hPSC line. Individual replicates plotted on bar graphs, mean ± S.D. One-way ANOVA with Dunnett test. \*\*\*$P = 0.0003$, \*\*\*\*$P = 0.0001$. $N = 4$ and 3 cultures for H9 and iSHH conditions, respectively. **c**, qRT-PCR analysis of *FOXA2*, a SHH target gene, during neural differentiation shows that iSHH expresses biologically active protein (iSHH −DOX vs. iSHH +DOX, \*\*$P = 0.0072$), at a level comparable to levels from hPSC-derived floorplate (iSHH −DOX vs. floorplate, $P = 0.0063$). *SHH* transcript expression is displayed in bottom panel (iSHH −DOX vs. iSHH +DOX, \*\*$P = 0.0026$). Individual replicates plotted on bar graphs, mean ± S.D. One-way ANOVA with Dunnett test. $N = 3$ differentiations for all conditions. **d**, Schematic of the method for generating forebrain organoids with a SHH protein gradient. Timeline and small molecules used for neural induction are shown. The specific timing of matrigel embedding can exhibit slight variation among differentiations. **e**, Visualization of SHH protein gradient using tyramide signal amplification (TSA). A line scan was used to quantify SHH protein signal. Graph shows mean ± 95% confidence interval. Intensity of SHH signal (*y* axis, green) normalized to maximum iSHH fluorescence. Origin (*x* axis) set to position of maximum iSHH fluorescence. −DOX, $N = 4$ spheroids, 1 batch; +DOX, $N = 6$ spheroids, 2 batches. **f**, Quantification of the distance at which the iSHH-organizer signal (ORG) and SHH protein signal (SHH) reach 25% of maximum intensity demonstrates that the SHH protein gradient extends beyond the limit of the organizer cells. Individual replicates plotted on bar graphs, mean ± S.D. Student two-tailed *t*-test. \*\*$P = 0.0022$. $N = 6$ spheroids, 2 batches. **g**, Schematic illustrating that PAX6 and NKX2.1 define dorsal and ventral forebrain, respectively. H9 organoids (H9) or SHH-organoids grown without doxycycline (−DOX) largely express PAX6 without detectable NKX2.1 expression, indicating dorsal identity. SHH-organoids grown in the presence of doxycycline (400 ng/ml, +DOX) suppress PAX6 and induce NKX2.1 near the iSHH organizer, indicating induction of ventral identity. Representative images are shown. H9, $N = 7$ organoids; −DOX, $N = 8$ organoids; SHH + DOX, $N = 11$ organoids. Samples are from at least 2 batches. **h**, Schematic illustrating that FOXG1 and OTX2 define anterior and posterior forebrain domains. H9 organoids (H9) or SHH-organoids grown without doxycycline (−DOX) largely express FOXG1 with only small amounts of OTX2 expression, indicating predominant telencephalic (anterior forebrain) identity. SHH-organoids grown in the presence of doxycycline (400 ng/ml, +DOX) suppress FOXG1 and induce OTX2 near the iSHH organizer, indicating induction of diencephalic (posterior forebrain) identity. Representative images are shown. H9, $N = 8$ organoids; −DOX, N = 8 organoids; +DOX, $N = 12$ organoids. Samples are from at least 2 batches. **i**, Schematic illustrating diencephalic expression of TCF7L2, SIX3, and *DKK1*. Organoids grown without doxycycline (−DOX) do not express TCF7L2 or SIX3. Organoids grown in the presence of doxycycline (400 ng/ml, +DOX) induce TCF7L2 and SIX3 at day 6. −DOX, $N = 6$ organoids; +DOX, $N = 6$ organoids. Samples are from at least 2 batches. **j**, Dose-dependent activation of *DKK1* by SHH. 0 ng/mL, $N = 8$ organoids; 80 ng/mL, $N = 8$ organoids; 400 ng/mL, $N = 6$ organoids; 2,000 ng/mL, $N = 6$ organoids. Organoids from two batches. Individual replicates plotted on bar graphs, mean ± S.D. One-way ANOVA, $P < 0.0001$, with Dunnett test. \*\*\*\*$P < 0.0001$. Scale bars: 200 μm.

subpallium-restricted identities[15,16]. Topographic patterning could also be achieved in the absence of matrigel (Supplementary Fig. 4b). SHH-spheroids differentiated in the absence of doxycycline expressed markers of dorsal-anterior forebrain, including PAX6 and FOXG1, with a small proportion of GSH2 expressing cells. These 3D cultures in the absence of doxycycline did not express the ventral identity genes NKX2.1 and NKX2.2 (Fig. 2d).

Interestingly, tissue cytoarchitecture differed between areas that are proximal (hypothalamic-like) and distal (telencephalic-like) to

the SHH source. At day 20, PAX6+ distal neuroepithelia acquired circular, rosette-like morphologies (Fig. 2e, inset), consistent with the self-organizing radial structures described for forebrain organoids[4,11]. In contrast, the NKX2.1+ proximal region contained many thin and highly extended neuroepithelia (Fig. 2e, inset) as observed previously for 3D structures of early hypothalamic lineages[10,30]. This appears to be restricted to diencephalic NKX2.1+ regions, as presumptive MGE domains (FOXG1+/NKX2.1+) typically acquired circular, rosette-like morphologies (Fig. 2c and Supplementary Fig. 4c).
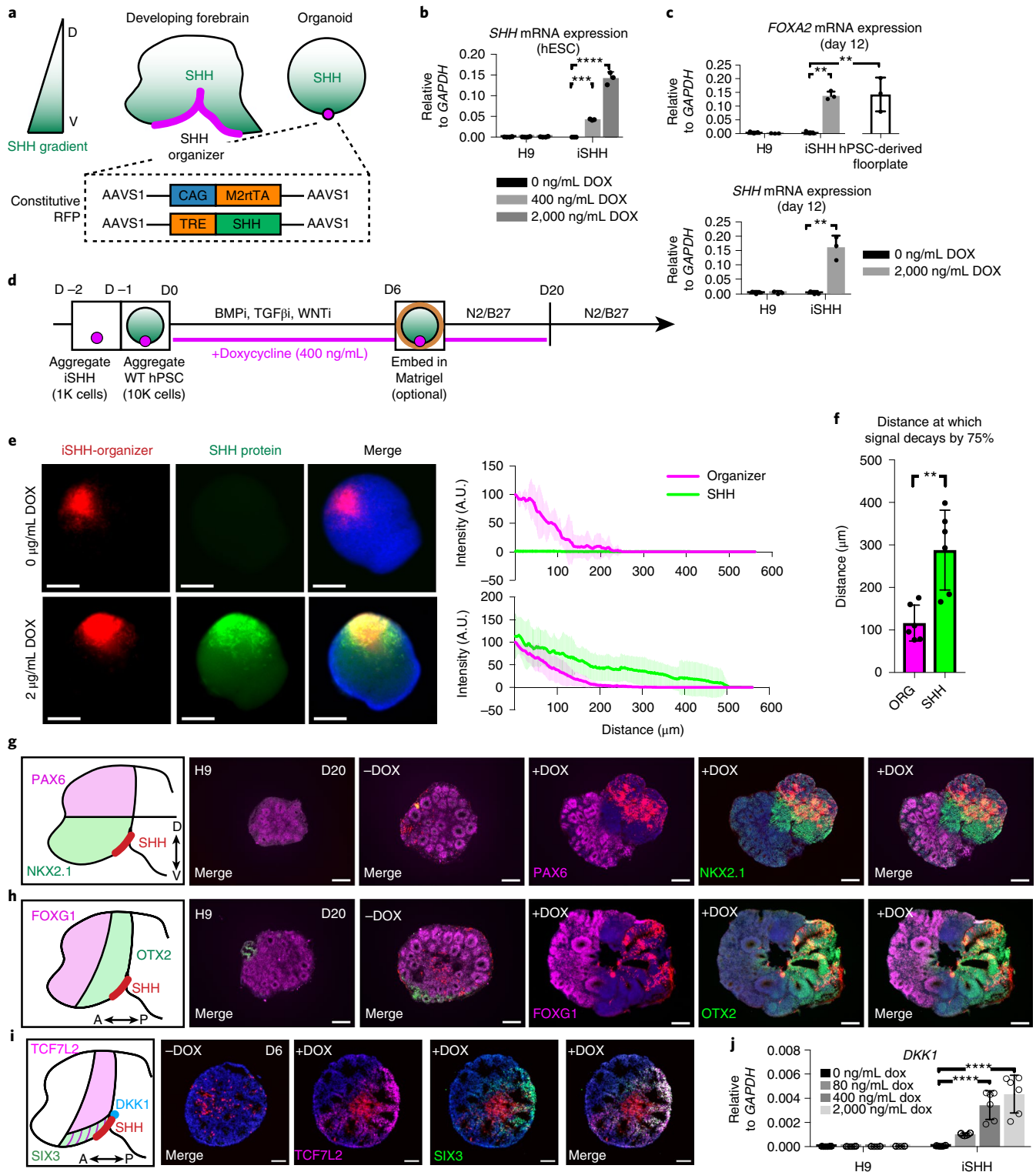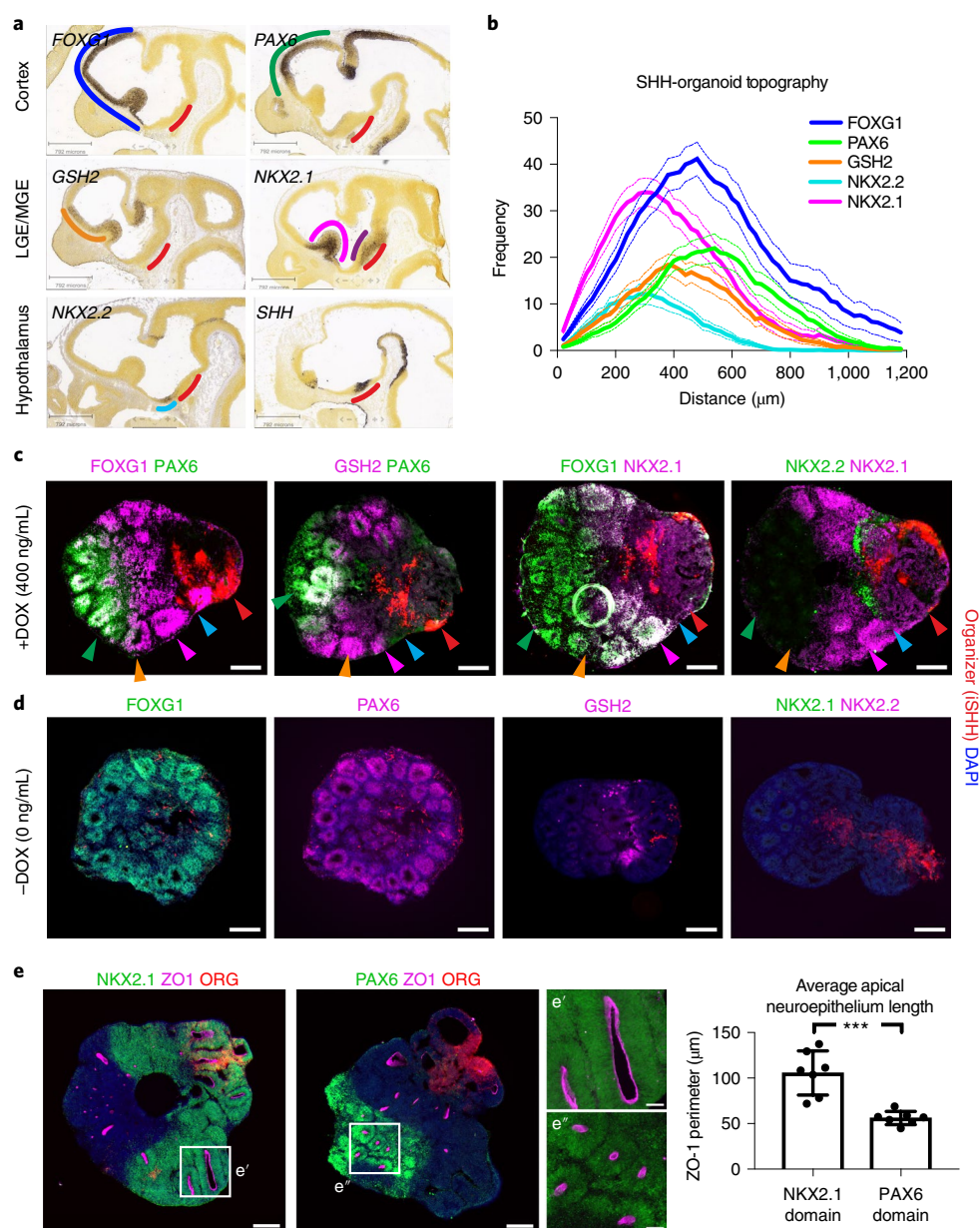
**Fig. 2 | *In vivo*-like topographic organization of major forebrain subdivisions in SHH-organoids. a**, *In situ* hybridization images depicting forebrain topography. The neocortex co-expresses *FOXG1* (blue) and *PAX6* (green), and is located distal to the *SHH* expression (red). The lateral ganglionic eminence (LGE) co-expresses *FOXG1* and *GSH2* (orange), and is just ventral to the neocortex. The medial ganglionic eminence (MGE) co-expresses *FOXG1* and *NKX2.1* (light purple), and is just ventral to the LGE. *NKX2.1* is also expressed in the ventro-posterior hypothalamus (dark purple), and is distinguished from the MGE by exclusion of *FOXG1* expression. The anterior hypothalamus expresses *NKX2.2* (cyan) and resides in the gap between MGE and Hypothalamic *NKX2.1* expression. *SHH* (red) is strongly expressed in the ventro-posterior hypothalamus, and is also weakly expressed in the ventral MGE. Images are from the 2008 Allen Institute for Brain Science. Allen Developing Mouse Brain Atlas. Available from developingmouse.brain-map.org. Scale bars, 792 μm. **b**, Quantification of position of regional domains in SHH-organoids (400 ng/ml doxycycline). Immunofluorescence signals of each regional marker are plotted as a function of distance from the iSHH organizer (see Methods and Supplementary Fig. 2 for details of quantification). Mean ± S.E.M. $N = 30$ organoids from 6 batches. **c**, Sections from a single organoid showing that SHH-organoids develop with *in vivo*-like topography. A neocortex-like domain that co-expresses FOXG1 and PAX6 is distal to the SHH organizer (red). A GSH2 domain is observed partially overlapping with and adjacent to the PAX6 domain. A FOXG1/NKX2.1 co-expression domain occupies an intermediate position between the neocortex-like domain and the SHH organizer. Finally, NKX2.2 and NKX2.1 are expressed in the FOXG1 negative territory, with NKX2.1 most proximal to the SHH organizer. Colors of arrowheads correspond to regional identities in panel 2a and delineate presumptive forebrain domains. Image is representative of quantification from **b**.
**d**, SHH-organoids grown without doxycycline treatment mainly express FOXG1 ($N = 6$ organoids, 2 batches) and PAX6 ($N = 6$ organoids, 2 batches), with some GSH2 expression ($N = 9$ organoids, 3 batches). No NKX2.1 or NKX2.2 is observed ($N = 10$ organoids, 3 batches). **e**, The length of ZO-1 apical neuroepithelia differs between PAX6+ and NKX2.1+ regions. PAX6+ regions contain circular, rosette-like neuroepithelia, while NKX2.1+ regions contain highly-extended neuroepithelia. High-magnification images correspond to insets. Quantification shows average neuroepithelium length in PAX6 versus NKX2.1 domains, mean ± S.D. Dots represent individual organoids. Student two-tailed *t*-test. ***$P = 0.0002$. $N = 7$ organoids, 2 batches for each condition. Scale bars: 200 μm (low magnification), 50 μm (high magnification).
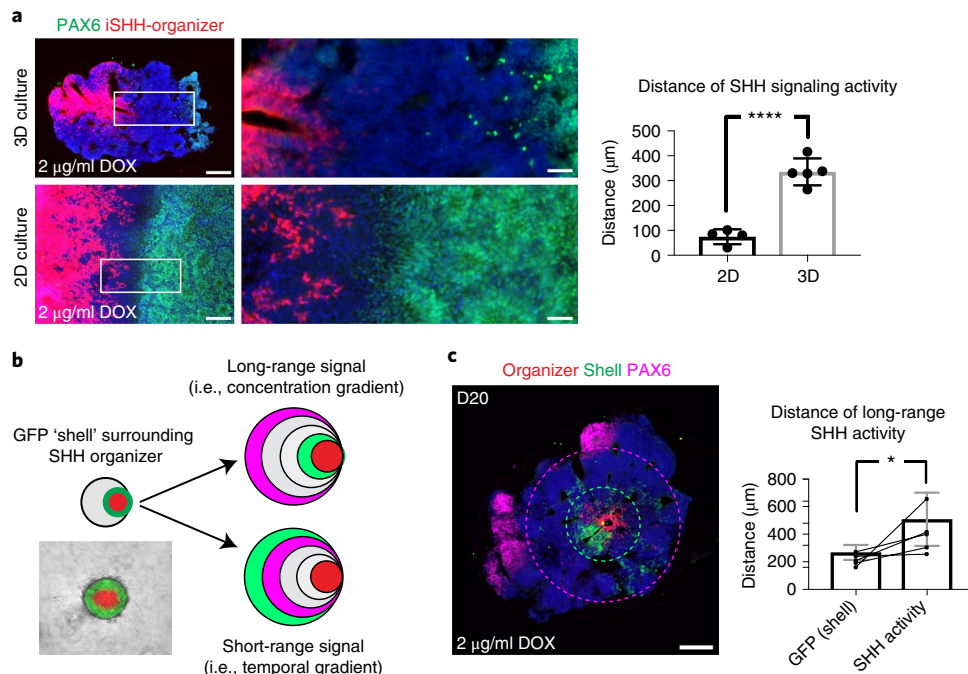
**Fig. 3 | Characterization of long-range SHH signaling mechanism. a**, Comparison of distance of SHH-signaling activity after 12 d of differentiation in 3D and 2D culture using 2 μg/ml doxycycline. In 3D culture, SHH acts over 335 ± 54 μm from the iSHH-organizer, assessed by suppression of PAX6 expression. In 2D culture, SHH acts 75 ± 31 μm from the iSHH-organizer cells. Insets show high-magnification images. Quantification shows mean ± S.D. Individual replicates are plotted on graphs. Student two-tailed *t*-test. ****$P < 0.0001$. 3D, $N = 5$ organoids, 2 batches; 2D, $N = 4$ differentiations. **b**, Depiction of experiment to distinguish between two theoretical mechanisms for long-range SHH activity in 3D culture. A shell of GFP-expressing hPSCs is embedded around the iSHH organizer (see Methods). A temporal model is supported if the all of SHH activity remains encapsulated within the GFP shell. A concentration-dependent model is supported if SHH activity extends past the GFP shell. **c**, After 20 d of differentiation in 2 μg/ml doxycycline, SHH activity is observed to extend past the GFP shell. The green dotted circle indicates the boundary of the GFP shell and the purple dotted circle indicates the boundary of the SHH activity, assessed by suppression of PAX6 activity. Quantifications show that the GFP shell extends 268 ± 24 μm from the iSHH-organizer, while SHH activity extends 508 ± 86 μm from the iSHH-organizer. Quantification shows mean ± S.D. Student two-tailed *t*-test. *$P = 0.028$. Individual replicates are plotted on graphs. $N = 5$ organoids, 2 batches. Scale bars: 200 μm (low magnification), 50 μm (high magnification).

Our data indicate that an asymmetric SHH cue enables the ordered patterning and topographical organization of brain regions without interfering in the self-organization process, which leads to the establishment of region-specific tissue microarchitectures. We term these 3D cultures SHH-organoids.

To explore the degree to which topography is maintained over time, we cultured SHH-organoids for up to 70 d. FOXG1+ and OTX2+ domains remained largely discrete at this stage, typically with the OTX2+ domain located proximal to the organizer, while the FOXG1+ domain was located distal to the organizer (Supplementary Fig. 5a). Radially organized PAX6, TBR2, TBR1 cerebral cortex-like tissue and DARPP32+ striatum-like tissue emerged in distal domains (Supplementary Fig. 5b–d), while hypothalamic-like tissue, expressing LHX6, OTP, POMC, and TH, was found in the immediate vicinity of the organizer cells (Supplementary Fig. 5d–f). In some instances organoid topography was more difficult to discern because the organizer seemed to have dispersed throughout the tissue. In addition, tissue necrosis in the center of those larger organoids may degrade organization over time.

The identity of LHX6+ cells including the presence of cortical interneurons was further defined by differentiating SHH-organoids using an *LHX6*-citrine hPSC line. As expected, LHX6+, putative hypothalamic precursors, emerge near the organizer, with some cells co-expressing NKX2.1 (Supplementary Fig. 6a). A subset of LHX6+ cells co-expresses FOXG1 (Supplementary Fig. 6b), while a subset is negative for FOXG1, suggesting the presence of both MGE and hypothalamic LHX6 lineages. Some FOXG1+/LHX6+ cells exhibit a leading-process morphology characteristic of migrating

interneurons (Supplementary Fig. 6c). Cells expressing SST, PV, or CR were observed in SHH-organoids (Supplementary Fig. 6d–f), suggesting the emergence of diverse interneuron populations. However, PV+ cells did not co-express LHX6 indicating that those PV+ cells many not represent cortical interneurons.

We next sought insight into the mechanisms by which a SHH signaling gradient establishes forebrain topography. Using the suppression of PAX6 as a read-out of SHH signaling activity, we compared the radial extent of PAX6 suppression in 2D versus 3D cultures. High-doxycycline conditions (2 μg/ml) were used in assessing SHH activity. In 3D cultures, we observe the suppression of PAX6 expression at an average distance of 335 ± 54 μm from the organizer tissue (Fig. 3a). Interestingly, this range is similar to the distances reported for SHH signaling *in vivo* based on studies across multiple tissues of the developing mouse or chick embryos[31–33]. However, in 2D cultures in which a similar 1:10 ratio of iSHH to wild-type cells is maintained, we saw suppression of PAX6 at much shorter average distances (75 ± 31 μm) from the SHH source tissue (Fig. 3a).

The observation that the range of SHH signaling activity is restricted in 2D raises the question how SHH establishes long-range gradients in 3D. We generated 2 theoretical models based on known mechanisms of SHH signaling *in vivo* (Fig. 3b). The first model is a concentration-dependent model. In this model, SHH signaling activity is determined by the local concentration of SHH morphogen, and is dependent on mechanisms that can transport SHH protein over long distances, such as diffusion, facilitated transport, or cell-to-cell relay[31,33–37]. The second model is a temporal model. In this model, SHH signaling is restricted to tissue immediately
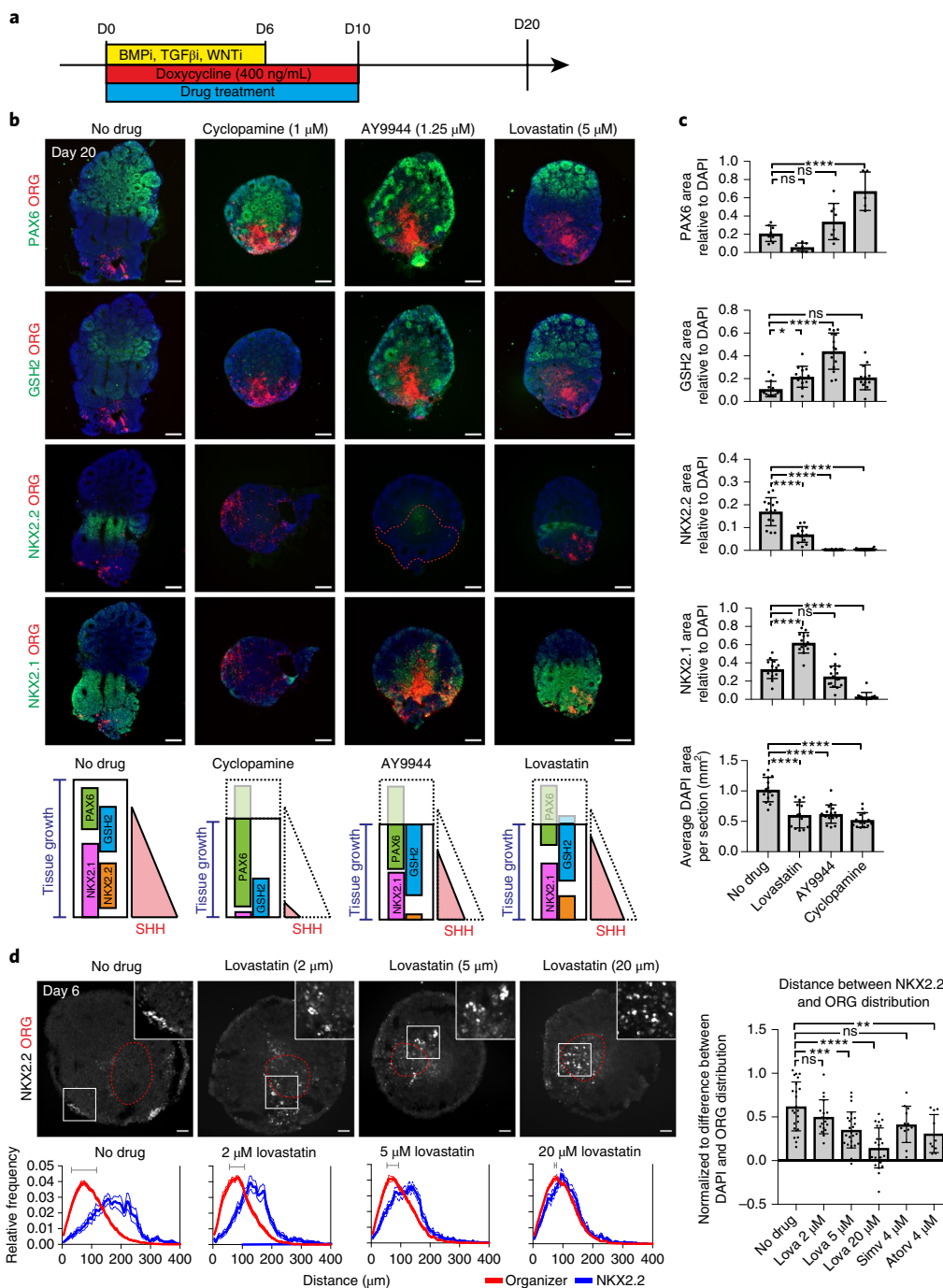
**Fig. 4 | Statins perturb tissue growth and SHH signaling. a**, Experimental design to test effect of statins on SHH-organoid development. **b**, Four distinct positional domains are identified in day 20 SHH-organoids (400 ng/ml doxycycline). SHH-organoids treated with cyclopamine (1 μM) largely express PAX6, with some GSH2 immunoreactivity, suggesting a near complete inhibition of SHH activity. SHH-organoids treated by AY9944 (1.25 μM) fail to induce NKX2.2 and only retain NKX2.1 expression in the immediate vicinity of the organizer, suggesting a strong reduction the range of SHH-signaling activity. SHH-organoids treated with lovastatin (5 μM) exhibit a moderate reduction in NKX2.2 induction, with a concomitant increase in the relative area of the GSH2 expression domain. Summary of drug phenotypes and potential impact on SHH signaling activity is depicted at bottom of panel. **c**, Quantification of area of each positional domain, relative to total area. Graph depicts mean ± S.D.; dots represent individual organoids. One-way ANOVA with Dunnett test for multiple comparisons. No drug $N = 8$–14 organoids; cyclopamine $N = 5$–14 organoids; AY9944 $N = 8$–16 organoids; lovastatin $N = 7$–13 organoids. Exact $N$ and batch values provided in Supplementary Table 2. *$P = 0.044$; ****$P = 0.0001$. **d**, Lovastatin produces a dose-dependent reduction in the distance at which NKX2.2 is induced from the organizer (red dotted boundary). Insets show NKX2.2 cells in boxed regions. Frequency histograms plot the relative distribution of organizer and NKX2.2+ cells as a function of distance from the center of the organizer. Graph depicts mean (solid line) ± S.E.M. (dotted line). Bar graphs quantify the average distance between the center of NKX2.2 and organizer distributions, illustrated by horizontal gray bars in frequency histograms. Bar graphs depict mean ± S.D., with dots representing individual organoids. One-way ANOVA with Dunnett test. **$P = 0.0023$; ***$P = 0.0005$; ****$P = 0.0001$. No drug $N = 23$ organoids, 4 batches; lovastatin (Lova) 2 μM $N = 18$ organoids, 3 batches; Lova 5 μM $N = 24$ organoids, 4 batches; Lova 20 μM $N = 23$ organoids, 4 batches; simvastatin (Simv) $N = 12$ organoids, 2 batches; atorvastatin (Atorv) $N = 10$ organoids, 2 batches. Scale bars: 200 μm (day 20); 50 μm (day 6).

adjacent to the source, which is relieved of SHH signaling as tissue grows away from the source[38]. Tissue that grows away from a SHH source will record a brief duration of signaling activity, while tissue that remains near the SHH source will record a long duration of signaling activity. This temporal model does not rely on transport of SHH over long distances.

To experimentally test these models, we embedded the iSHH organizer within a circumscribed ring of GFP-expressing hPSCs. This was achieved by sequential plating of 1,000 iSHH cells, followed by 1,000 GFP cells 8 h later, followed by 10,000 H9 cells the next day. We reasoned that if the activity of SHH extends past the GFP boundary, this would support a long-range concentration-dependent mechanism. On the other hand, if the GFP boundary expands coincident with the extent of SHH activity, this would support a temporal model in which tissue growth rather than protein transport establishes long-range SHH activity (Fig. 3b). After growing SHH-GFP-organoids for 20 d in doxycycline (2 µg/ml), we observed that the GFP-expressing cells stayed within $285 \pm 44 \, \mu m$ to the SHH organizer cells. The activity of SHH, determined as suppression of PAX6 expression, extended to $430 \pm 96 \, \mu m$, past the green boundary (Fig. 3c). These data provide evidence for a concentration-dependent signaling mechanism in which SHH protein is transported long distances away from producing cells. Still, because the long-range SHH signal degrades in 2D culture while a short-range signal persists, our data do not exclude the possibility of a concurrent short-range signaling mechanism in which the activity SHH is restricted to the immediate vicinity of producing cells. In fact, during limb patterning, SHH is known to act by both short- and long-range signaling mechanisms, and such an interplay of short- and long-range signaling may also be critical during forebrain development[29,39–41].

The reproducible topography of SHH-organoids might make them suitable as a tool to study signaling mechanisms during early forebrain patterning. Cholesterol is integrally linked to the SHH pathway in many ways. Cholesterol is an agonist of the smoothened receptor[42,43]. SHH long-range signaling is dependent on the cholesterol post-translational modification of SHH[34,35,44], cholesterol rich lipid rafts[36,45,46], and can be facilitated by cholesterol-rich macromolecular soluble complexes[47,48].

To explore the multifaceted relationship of cholesterol to SHH signaling, we treated SHH-organoids (400 ng/ml doxycycline) from days 0–10 with small molecules that inhibit cholesterol synthesis at different points along the biosynthetic pathway (Fig. 4a). AY9944 is a specific inhibitor of 7-dehydrocholesterol reductase (DHCR7), which facilitates the terminal step of cholesterol synthesis. Lovastatin is an inhibitor of HMG-CoA reductase, an early step in cholesterol biosynthesis. Cyclopamine, a Smoothened antagonist that blocks all SHH activity, was used as a control. At day 20 in the no drug condition, SHH-organoids established distinct positional domains marked by the expression of PAX6, GSH2, NKX2.2, and NKX2.1 at discrete distances from the SHH-organizer (Fig. 4b). As expected, SHH-organoids grown in the presence of cyclopamine (1 µM[49]) were nearly uniform for PAX6 expression, with some GSH2 expression, consistent with a near complete inhibition of SHH signaling activity (Fig. 4b,c). AY9944 (1.25 µM[50]) treatment reduced the efficacy and range of SHH signaling activity, shifting the organoid to a more dorsal identity. NKX2.2 induction was largely blocked, while cells just adjacent to the organizer expressed GSH2 and PAX6 (Fig. 4b,c). Lovastatin (5 µM[50]) treatment caused similar, but milder effects, than AY9944. There was a partial block in NKX2.2 induction, with concomitant increase in GSH2 expression (Fig. 4b,c), consistent with a dorsal shift and reduction in the efficacy and range of SHH signaling activity. Notably, the organizer cells retained diencephalic NKX2.1 expression in the presence of AY9944 or lovastatin but not cyclopamine (Supplementary Fig. 7a), suggesting that inhibition of cholesterol synthesis has minimal impact on local SHH activity.

In addition to the effects on patterning, all drugs affected organoid growth. Overall organoid size was reduced in all treatment conditions (Fig. 4b,c). However, AY9944 and lovastatin did not reduce the size of the organizer itself (Supplementary Fig. 7b), consistent with the interpretation that cholesterol-synthesis inhibition has differential effects on local and long-range SHH activity. To dissociate growth and patterning phenotypes, we analyzed organoids at day 6, during the early stages of SHH patterning, and prior to the major phase of tissue growth (which occurs after matrigel embedding). We used NKX2.2, a direct target of GLI[51], as a read-out of SHH signaling activity. By measuring the distance at which NKX2.2 is expressed from the SHH producing cells, we could infer the distance of SHH signaling activity. Lovastatin reduced the distance at which NKX2.2 is induced from the organizer in a dose-dependent manner (Fig. 4d). AY9944 strongly inhibited NKX2.2 induction at all concentrations tested (Supplementary Fig. 7c). Neither AY9944 nor lovastatin grossly perturbed processing of SHH peptide length (Supplementary Fig. 7d). Together, these data support a model in which inhibition of cholesterol synthesis by lovastatin or AY9944 result in a complex developmental phenotype characterized by impaired growth and a reduction in the range of SHH signaling activity, though perhaps in distinct ways.

This study reveals that an asymmetric morphogenetic cue provides positional information from which *in vivo*-like topography can emerge in brain organoids. Furthermore, we present evidence that SHH uses a long-range signaling mechanism during forebrain organoid development, recapitulating its *in vivo* behavior[40]. The emergence of long-range activity in 3D that is not present in 2D cultures highlights the importance of tissue geometry on the spatial dynamics of signaling activity.

The strategy of generating topographically patterned organoids allowed us to investigate how alterations in cholesterol metabolism perturb SHH-dependent patterning. Our data suggest that while both AY9944 and lovastatin impair SHH-dependent patterning, they may do so in different ways. AY9944 has previously been shown to block Smoothened activation[50], consistent with the reduction in NKX2.2 induction at day 6 (Supplementary Fig. 7c). On the other hand, lovastatin reduced the range of SHH signaling at day 6 without reducing the intensity of signaling. While future studies are required to determine mechanism of action, there are multiple possible explanations for this observation. First, statin treatment could disrupt lipid raft integrity[52–56], which is required for long-range hedgehog signaling[46] and perhaps SHH oligomerization at the membrane[57,58]. Second, statins could lead to removal of the C-terminal SHH cholesterol modification, which is required for long-range signaling[34,35,44]. While it is unlikely that statins block the initial cholesterylation of SHH during auto-cleavage[59], SHH can subsequently lose its C-terminal cholesterol through proteolytic cleavage, or 'shedding', at the cell membrane[60]. Notably, disruption of lipid rafts by sterol-reduction, either with statins or methyl-β-cyclodextrin, increases shedding of multiple membrane-associated proteins, including SHH[52,53,60]. Third, statin treatment could reduce the formation of cholesterol-rich multimeric SHH complexes involved in long-range transport[47,48]. Finally, it is possible that statins perturb SHH patterning through isoprenoid pathway inhibition or off-target effects given the high concentration of drug used. Statins have been reported to be associated with fetal maldevelopment, including holoprosencephaly, in a small number of cases[61]. Our data suggest that some of these cases may be due to impaired SHH signaling, although caution must be exercised given the high concentration of statin used in our experiments (5 µM) compared to the typical plasma concentration of statin (15–20 nM)[62].

A key feature of the patterning strategy presented here is the establishment of well-ordered positional domains during early organoid development. In future studies it will be important to

determine the extent to which the topography of these domains can be retained during long-term *in vitro* culture for the study of region-specific neuronal diversity as well as connectivity and function. It is possible that additional tissue engineering approaches will be required to facilitate the maintenance of topography over time and to prevent increasing cell mixing or inappropriate migration, processes that could blur the boundaries between positional domains over time. For example, manipulating soluble ECM components has been used to improve the maintenance of radially organized structures within organoids over time[63].

For disease modeling, current organoid technologies have been successful at modeling cortical progenitor dynamics that ultimately result in changes in brain size. Pre-patterning and fusion of pallial- and subpallial-specific spheroids have been used to study specific phenotypes related to cortical interneuron migration and connectivity[16]. The establishment of forebrain topography in organoids shown here opens the possibility of studying a wide range of phenotypes in a single organoid system. In particular, it would be interesting to study complex neurodevelopmental diseases that have been hypothesized to alter or derive from regional specification during forebrain patterning, including autism[64], epilepsy[65], or suprasellar pediatric gliomas[66]. In the future it will important to develop strategies such as bio-engineering approaches to reduce the variability of topography in long-term cultures. Finally, it will be exciting to test whether our strategy could be used as a general approach to establish topographies across all regions of the CNS beyond the forebrain.

## Online content

## References

1. Kelava, I. & Lancaster, M. A. Stem cell models of human brain development. *Cell Stem Cell* **18**, 736–748 (2016).
2. Sasai, Y., Eiraku, M. & Suga, H. In vitro organogenesis in three dimensions: self-organising stem cells. *Development* **139**, 4111–4121 (2012).
3. Lancaster, M. A. & Knoblich, J. A. Organogenesis in a dish: modeling development and disease using organoid technologies. *Science* **345**, 1247125 (2014).
4. Lancaster, M. A. et al. Cerebral organoids model human brain development and microcephaly. *Nature* **501**, 373–379 (2013).
5. Quadrato, G., Brown, J. & Arlotta, P. The promises and challenges of human brain organoids as models of neuropsychiatric disease. *Nat. Med.* **22**, 1220–1228 (2016).
6. Renner, M. et al. Self-organized developmental patterning and differentiation in cerebral organoids. *EMBO J.* **36**, 1316–1329 (2017).
7. O'Leary, D. D., Chou, S. J. & Sahara, S. Area patterning of the mammalian cortex. *Neuron* **56**, 252–269 (2007).
8. Sagner, A. & Briscoe, J. Morphogen interpretation: concentration, time, competence, and signaling dynamics. *Wiley Interdiscip. Rev. Dev. Biol.* **6**, https://doi.org/10.1002/wdev.271 (2017).
9. Eiraku, M. et al. Self-organizing optic-cup morphogenesis in three-dimensional culture. *Nature* **472**, 51–56 (2011).
10. Suga, H. et al. Self-formation of functional adenohypophysis in three-dimensional culture. *Nature* **480**, 57–62 (2011).
11. Kadoshima, T. et al. Self-organization of axial polarity, inside-out layer pattern, and species-specific progenitor dynamics in human ES cell-derived neocortex. *Proc. Natl Acad. Sci. USA* **110**, 20284–20289 (2013).
12. Jo, J. et al. Midbrain-like organoids from human pluripotent stem cells contain functional dopaminergic and neuromelanin-producing neurons. *Cell Stem Cell* **19**, 248–257 (2016).
13. Muguruma, K., Nishiyama, A., Kawakami, H., Hashimoto, K. & Sasai, Y. Self-organization of polarized cerebellar tissue in 3D culture of human pluripotent stem cells. *Cell Rep.* **10**, 537–550 (2015).
14. Qian, X. et al. Brain-region-specific organoids using mini-bioreactors for modeling ZIKV exposure. *Cell* **165**, 1238–1254 (2016).
15. Bagley, J. A., Reumann, D., Bian, S., Levi-Strauss, J. & Knoblich, J. A. Fused cerebral organoids model interactions between brain regions. *Nat. Methods* **14**, 743–751 (2017).
16. Birey, F. et al. Assembly of functionally integrated human forebrain spheroids. *Nature* **545**, 54–59 (2017).
17. Xiang, Y. et al. Fusion of Regionally Specified hPSC-Derived Organoids Models Human Brain Development and Interneuron Migration. *Cell Stem Cell* **21**, 383–398.e387 (2017).
18. Lupo, G., Harris, W. A. & Lewis, K. E. Mechanisms of ventral patterning in the vertebrate nervous system. *Nat. Rev. Neurosci.* **7**, 103–114 (2006).
19. Jessell, T. M. Neuronal specification in the spinal cord: inductive signals and transcriptional codes. *Nat. Rev. Genet.* **1**, 20–29 (2000).
20. Fattahi, F. et al. Deriving human ENS lineages for cell therapy and drug discovery in Hirschsprung disease. *Nature* **531**, 105–109 (2016).
21. Gonzalez, F. et al. An iCRISPR platform for rapid, multiplexable, and inducible genome editing in human pluripotent stem cells. *Cell Stem Cell* **15**, 215–226 (2014).
22. Shiraishi, A., Muguruma, K. & Sasai, Y. Generation of thalamic neurons from mouse embryonic stem cells. *Development* **144**, 1211–1220 (2017).
23. Merchan, P., Bardet, S. M., Puelles, L. & Ferran, J. L. Comparison of pretectal genoarchitectonic pattern between quail and chicken embryos. *Front. Neuroanat.* **5**, 23 (2011).
24. Oliver, G. et al. Six3, a murine homologue of the sine oculis gene, demarcates the most anterior border of the developing neural plate and is expressed during eye development. *Development* **121**, 4045–4055 (1995).
25. Shinya, M., Eschbach, C., Clark, M., Lehrach, H. & Furutani-Seiki, M. Zebrafish Dkk1, induced by the pre-MBT Wnt signaling, is secreted from the prechordal plate and patterns the anterior neural plate. *Mech. Dev.* **98**, 3–17 (2000).
26. Houart, C. et al. Establishment of the telencephalon during gastrulation by local antagonism of Wnt signaling. *Neuron* **35**, 255–265 (2002).
27. Kiecker, C. & Niehrs, C. A morphogen gradient of Wnt/beta-catenin signalling regulates anteroposterior neural patterning in Xenopus. *Development* **128**, 4189–4201 (2001).
28. Maroof, A. M. et al. Directed differentiation and functional maturation of cortical interneurons from human embryonic stem cells. *Cell Stem Cell* **12**, 559–572 (2013).
29. Blaess, S., Szabo, N., Haddad-Tovolli, R., Zhou, X. & Alvarez-Bolado, G. Sonic hedgehog signaling in the development of the mouse hypothalamus. *Front. Neuroanat.* **8**, 156 (2014).
30. Merkle, F. T. et al. Generation of neuropeptidergic hypothalamic neurons from human pluripotent stem cells. *Development* **142**, 633–643 (2015).
31. Briscoe, J., Chen, Y., Jessell, T. M. & Struhl, G. A hedgehog-insensitive form of patched provides evidence for direct long-range morphogen activity of sonic hedgehog in the neural tube. *Mol. Cell* **7**, 1279–1291 (2001).
32. Honig, L. S. Positional signal transmission in the developing chick limb. *Nature* **291**, 72–73 (1981).
33. Fan, C. M. & Tessier-Lavigne, M. Patterning of mammalian somites by surface ectoderm and notochord: evidence for sclerotome induction by a hedgehog homolog. *Cell* **79**, 1175–1186 (1994).
34. Zeng, X. et al. A freely diffusible form of Sonic hedgehog mediates long-range signalling. *Nature* **411**, 716–720 (2001).
35. Lewis, P. M. et al. Cholesterol modification of sonic hedgehog is required for long-range signaling activity and effective modulation of signaling by Ptc1. *Cell* **105**, 599–612 (2001).
36. Chen, M. H., Li, Y. J., Kawakami, T., Xu, S. M. & Chuang, P. T. Palmitoylation is required for the production of a soluble multimeric Hedgehog protein complex and long-range signaling in vertebrates. *Genes Dev.* **18**, 641–659 (2004).
37. Sanders, T. A., Llagostera, E. & Barna, M. Specialized filopodia direct long-range transport of SHH during vertebrate tissue patterning. *Nature* **497**, 628–632 (2013).
38. Harfe, B. D. et al. Evidence for an expansion-based temporal Shh gradient in specifying vertebrate digit identities. *Cell* **118**, 517–528 (2004).
39. Zhang, Y. & Alvarez-Bolado, G. Differential developmental strategies by Sonic hedgehog in thalamus and hypothalamus. *J. Chem. Neuroanat.* **75**, 20–27 (2016).
40. McGlinn, E. & Tabin, C. J. Mechanistic insight into how Shh patterns the vertebrate limb. *Curr. Opin. Genet. Dev.* **16**, 426–432 (2006).
41. Ericson, J. et al. Sonic hedgehog induces the differentiation of ventral forebrain neurons: a common signal for ventral patterning within the neural tube. *Cell* **81**, 747–756 (1995).
42. Huang, P. et al. Cellular cholesterol directly activates Smoothened in Hedgehog signaling. *Cell* **166**, 1176–1187 e1114 (2016).
43. Byrne, E. F. X. et al. Structural basis of Smoothened regulation by its extracellular domains. *Nature* **535**, 517–522 (2016).
44. Tian, H., Jeong, J., Harfe, B. D., Tabin, C. J. & McMahon, A. P. Mouse Disp1 is required in sonic hedgehog-expressing cells for paracrine activity of the cholesterol-modified ligand. *Development* **132**, 133–142 (2005).

45. Rietveld, A., Neutz, S., Simons, K. & Eaton, S. Association of sterol- and glycosylphosphatidylinositol-linked proteins with Drosophila raft lipid microdomains. *J. Biol. Chem.* **274**, 12049–12054 (1999).

46. Katanaev, V. L. et al. Reggie-1/flotillin-2 promotes secretion of the long-range signalling forms of Wingless and Hedgehog in Drosophila. *EMBO J.* **27**, 509–521 (2008).

47. Panakova, D., Sprong, H., Marois, E., Thiele, C. & Eaton, S. Lipoprotein particles are required for Hedgehog and Wingless signalling. *Nature* **435**, 58–65 (2005).

48. Palm, W. et al. Lipoproteins in Drosophila melanogaster–assembly, function, and influence on tissue lipid composition. *PLoS Genet.* **8**, e1002828 (2012).

49. Gaspard, N. et al. An intrinsic mechanism of corticogenesis from embryonic stem cells. *Nature* **455**, 351–357 (2008).

50. Blassberg, R., Macrae, J. I., Briscoe, J. & Jacob, J. Reduced cholesterol levels impair Smoothened activation in Smith-Lemli-Opitz syndrome. *Hum. Mol. Genet.* **25**, 693–705 (2016).

51. Lei, Q. et al. Wnt signaling inhibitors regulate the transcriptional response to morphogenetic Shh-Gli signaling in the neural tube. *Dev. Cell* **11**, 325–337 (2006).

52. von Tresckow, B. et al. Depletion of cellular cholesterol and lipid rafts increases shedding of CD30. *J. Immunol.* **172**, 4324–4331 (2004).

53. Murai, T. et al. Low cholesterol triggers membrane microdomain-dependent CD44 shedding and suppresses tumor cell migration. *J. Biol. Chem.* **286**, 1999–2007 (2011).

54. Kirsch, C., Eckert, G. P. & Mueller, W. E. Statin effects on cholesterol micro-domains in brain plasma membranes. *Biochem. Pharmacol.* **65**, 843–856 (2003).

55. Hering, H., Lin, C. C. & Sheng, M. Lipid rafts in the maintenance of synapses, dendritic spines, and surface AMPA receptor stability. *J. Neurosci.* **23**, 3262–3271 (2003).

56. Zhuang, L., Kim, J., Adam, R. M., Solomon, K. R. & Freeman, M. R. Cholesterol targeting alters lipid raft composition and cell survival in prostate cancer cells and xenografts. *J. Clin. Invest.* **115**, 959–968 (2005).

57. Therond, P. P. Release and transportation of Hedgehog molecules. *Curr. Opin. Cell Biol.* **24**, 173–180 (2012).

58. Vyas, N. et al. Nanoscale organization of hedgehog is essential for long-range signaling. *Cell* **133**, 1214–1227 (2008).

59. Cooper, M. K., Porter, J. A., Young, K. E. & Beachy, P. A. Teratogen-mediated inhibition of target tissue response to Shh signaling. *Science* **280**, 1603–1607 (1998).

60. Dierker, T., Dreier, R., Petersen, A., Bordych, C. & Grobe, K. Heparan sulfate-modulated, metalloprotease-mediated sonic hedgehog release from producing cells. *J. Biol. Chem.* **284**, 8013–8022 (2009).

61. Edison, R. J. & Muenke, M. Central nervous system and limb anomalies in case reports of first-trimester statin exposure. *N. Engl. J. Med.* **350**, 1579–1582 (2004).

62. Bellosta, S., Paoletti, R. & Corsini, A. Safety of statins: focus on clinical pharmacokinetics and drug interactions. *Circulation* **109**, III50–57 (2004).

63. Lancaster, M. A. et al. Guided self-organization and cortical plate formation in human brain organoids. *Nat. Biotechnol.* **35**, 659–666 (2017).

64. Mariani, J. et al. FOXG1-dependent dysregulation of GABA/glutamate neuron differentiation in autism spectrum disorders. *Cell* **162**, 375–390 (2015).

65. Cobos, I. et al. Mice lacking Dlx1 show subtype-specific loss of interneurons, reduced inhibition and epilepsy. *Nat. Neurosci.* **8**, 1059–1068 (2005).

66. Fontebasso, A. M. et al. Recurrent somatic mutations in ACVR1 in pediatric midline high-grade astrocytoma. *Nat. Genet.* **46**, 462–466 (2014).

## Author contributions

G.Y.C.: Conception and study design, Organoid protocol development, hPSC cell line engineering, differentiation and characterization assays and writing of manuscript. L.S.: Conception and study design, data analysis and interpretation, writing of manuscript. J.J.A.: SHH protein analysis. M.D.R.: SHH protein analysis. J.T. SHH protein analysis, hPSC cell line engineering. R.M.W.: Organoid protocol development and analysis. D.C.: cell line engineering.

## Competing interests

The Memorial Sloan-Kettering Cancer Center has filed a provisional patent application (US PRO 62/538,350) on the methods described in the manuscript with G. Cederquist and L. Studer listed as inventors. L.S. is a scientific co-founder of Bluerock Therapeutics.

## Additional information

**Supplementary information** is available for this paper at https://doi.org/10.1038/s41587-019-0085-3.

**Reprints and permissions information** is available at www.nature.com/reprints.

**Correspondence and requests for materials** should be addressed to L.S.

**Publisher's note:** Springer Nature remains neutral with regard to jurisdictional claims in published maps and institutional affiliations.

## Methods

**hPSC maintenance and monolayer differentiation.** hPSC (H9 and derivatives (EF1α::GFP (GFP), EF1 α::RFP; TRE-SHH (iSHH), MEL1, HUES6, HUES8, *LHX6*-citrine[67]) and iPSC (J1 and 348) were maintained with Essential 8 medium or Essential 8 flex (E8, Thermo, A15117001 or A28558501) in feeder-free conditions on vitronectin (VTN-N) substrate (Thermo, A14700). hPSCs were passaged as clumps with EDTA solution (0.5 M EDTA/PBS). For neural monolayer differentiation, hPSCs were dissociated to single cells and plated on matrigel substrate (BD Biosciences, 354234) in E8 at a density of 250,000 cells/cm² in the presence of ROCK inhibitor (Y-27632, 10 μM, Tocris 1254) (day −1). From days 0 to 7, cells were cultured in Essential 6 medium (E6, Thermo, A1516401) in the presence of TGFβ and BMP inhibitors (LDN193189, 100 nM, Stem Cell Technologies, 72142; SB431542, 10 μM, Tocris, 1614). From days 7 to 12, cells were cultured in E6 alone. Floorplate was specified by addition of SHH (200 ng/ml, R&D Systems 464-SH) and CHIR99021 (0.7 μM, Tocris 4423). Medium was changed every day during the differentiation.

**SHH inducible line.** The iSHH hPSC was generated according to a previously described gene targeting strategy[21]. Briefly, two donor constructs were targeted to the first intron of the *AAVS1* locus using TALEN-facilitated homologous recombination. One construct contained a constitutively expressed reverse tetracycline transactivator (M2rtTA) and the second construct contained a tetracycline inducible (TRE) SHH cassette. The SHH cassette was generated using full length human SHH cDNA (Genecopoeia T1004). Targeting was performed in a constitutive RFP expressing line (WA09 derived, EF1α::RFP) so iSHH cells could be visualized[20].

**SHH-spheroid aggregation.** 1,000 iSHH cells were dissociated to single cell and aggregated in low-attachment round bottom microwells for 24 h in the presence of ROCK inhibitor (Y-27632, 10 μM) and WNT inhibitor (XAV939, 5 μM). For Fig. 3c, the GFP boundary was established by first plating iSHH cells and allowing them to aggregate for 8 h. 1,000 GFP cells were then plated on top and allowed to aggregate overnight. The next day, 10,000 wildtype H9 hPSCs were dissociated to single cell and allowed to aggregate on top of the iSHH cells, in E8 medium with ROCK inhibitor (Y-27632, 10 μM) and WNT inhibitor (XAV939, 5 μM, Tocris 3748).

**SHH-organoid differentiation.** SHH-spheroids were cultured in E6 with 3-inhibitors (LDN193189, 100 nM; SB431542, 10 μM; XAV939, 5 μM) plus doxycycline (400 ng/mL) until spheroid tissue began to brighten and have smooth edges, typically 6–8 d. SHH-spheroids were then embedded in matrigel drops and cultured in a N2/B27 based organoid medium as previously described[68], except NeuroBrew B21 (Miltenyi Biotec) was substituted for B27. SHH-spheroids were moved to an orbital shaker once formation of translucent, neuroepithelial buds was observed, typically 4–7 d after embedding. Organoids that failed to form translucent, neuroepithelial buds were discarded. Half of the medium was changed every other day.

**Histology and immunocytochemistry.** Day 20 organoids were fixed in 4% PFA overnight at 4 °C, and washed three times with PBS the next day. After fixation, tissue was cryoprotected in 30% sucrose/PBS and sectioned at 30 μm on a cryostat (Leica 3050 S). Sections were blocked for 30 min in 10% FBS, 1% BSA, 0.3% triton in PBS, and incubated as floating section in primary antibody overnight (see Supplementary Table 1). The next day, sections were washed with PBS and incubated as floating section in secondary antibody for 3 h at room temperature. Day 6 organoids were fixed in 4% PFA for 2 h at 4 °C, and washed three times with PBS. After fixation, tissue was cryoprotected in 30% sucrose/PBS and sectioned at 20 μm and mounted directly onto slides prior to immunofluorescence assays.

**Quantification of organoid patterning and SHH activity.** Organoid topography was quantified by first dividing each image into a grid of 20 μm × 20 μm squares (day 20 analysis) or 5 μm × 5 μm squares (day 6 analysis) that form a Cartesian coordinate grid. Each square is a discrete region of interest (ROI) that is associated with an *x* and *y* coordinate. The origin of the grid was calculated for each image as the "center of mass" of the iSHH-organizer cells: $CM_x = \Sigma\, m_i x_i / M$ and $CM_y = \Sigma\, m_i y_i / M$, where *m* is the gray value intensity of iSHH cells for individual ROIs, *x* or *y* is the coordinate, and *M* is the total intensity for all ROIs, and the sum includes all *x* or *y* coordinates in the image. Next, ROI's that were positive for expression of a given protein (e.g. PAX6) were defined by thresholding staining intensity and determining ROIs with positive immunoreactivity. The linear distance from the origin to each ROI ($sqrt((ROI_x - CM_x)^2 + (ROI_y - CM_y)^2)$) was calculated. We attempted to analyze every sixth section for each regional marker per organoid (2–5 sections typically), thus sampling the organoids in 150 μm intervals using uniform random sampling.

In Figs. 2c and 4d ROI frequencies are plotted as a function of distance from the center of mass. In Fig. 3c the GFP shell distance is defined as the radial distance from the center of mass at which the ratio of GFP ROIs / DAPI ROIs drops below 35%. The SHH-activity distance is the radial distance from the

center of mass to the edge of the PAX6-negative territory, defined as the distance at which the ratio of PAX6-negative ROIs / DAPI ROIs dropped below 95% (PAX6-negative ROIs were obtained by subtracting PAX6 thresholded pixels from DAPI thresholded pixels). The 35 and 95% parameters were determined prior to analysis as accurately cut off values by comparing with manual distance measurements. Area measurements in Fig. 4b are determined by calculating the number of positive ROIs positive for a given gene (e.g. PAX6) divided by the ROIs positive for DAPI. Exclusion criteria for analysis: 1) organoid batches that failed to induce FOXG1 expression (Supplementary Fig. 2b), 2) organoids containing a split organizer, in which we observe two independent patterning centers (Supplementary Fig. 2c), 3) Sections that lacked organizer cells, a center of mass could not be defined, and 4) sections that had large necrotic centers as this could confound distance analysis.

The distance of SHH patterning activity in Fig. 3a was obtained by measuring the distance of lines from the edge of PAX6 territory to the nearest organizer cells. At least 5 lines were measured per section. All quantifications were performed using ImageJ.

Microscopy was performed using a standard inverted epifluorescence microscope (Olympus IX71 or Zeiss Axio Observer). Images were acquired using Cell Sens (Olympus) or Zen Pro (Zeiss) software. Min, max and gamma (midtone) adjustments were applied uniformly to images during processing with Adobe Photoshop Creative Cloud.

**RNA extraction and RT-PCR.** RNA was extracted using TRIzol (Invitrogen, 15596026) followed by chloroform extraction. RNA was precipitated in isopropanol and resuspended in nuclease free ddH2O. cDNA synthesis was performed using 1 μg of RNA (iScript, Bio-Rad, 1708840). RT-PCR was performed with EvaGreen Supermix (Bio-Rad, 1725202). Three to four individual samples were combined into a single replicate when collecting RNA from spheroids.

**Visualization of SHH protein gradient.** SHH-spheroids were fixed in 4% PFA for 6 h at 4 C, then washed three times in PBS. Standard immunocytochemistry was performed on wholemount SHH-spheroids using anti-SHH primary antibody (1:100, clone 5E1, DSHB). Secondary antibody was amplified using a tyramide signal amplification kit (Thermo, B40941). Fluorescence labeled spheroids were visualized using an inverted epifluorescence microscope. Gradients were quantified using line scans that transected the organizer tissue. Quantifications were performed using ImageJ.

**Cell-based SHH palmitoylation assay.** Synthesis of [I^125]iodopalmitate was carried out as previously described[69–71]. iSHH hPSC were dissociated to single cell and seeded as a confluent monolayer on matrigel substrate at a density of 250,000 cells / cm² and differentiated for 9 d in E6 with LDN193189, (100 nM) and SB431542 (10 μM) at increasing concentrations of doxycycline (0, 125, 250, 500, 1000, 2000 ng/ml). On day 9, iSHH cells were incubated for 1 h at 37 °C with DMEM containing 2% dialyzed FBS and then labeled for 4 h with 10 μCi of [I^125] iodopalmitate. The cells were lysed and subjected to immunoprecipitation with an anti-SHH antibody, and the immunoprecipitates were diluted in 100 μl of 2× SDS-PAGE sample buffer containing 10 mM DTT. The samples were analyzed on a 12.5% SDS-PAGE gel, followed by phosphorimaging on a Typhoon FLA-7000 phosphorimager. An aliquot of each immunoprecipitate was analyzed for SHH protein expression by Western blotting.

**SHH western blot.** Cells were harvested and washed with PBS. Cell pellets were lysed in RIPA buffer (Boston Bioproducts Inc. NC9517624) supplemented with protease inhibitors (Thermo 78425) and ran through a syringe several times. Lysate was incubated for 30 min on ice and then centrifuged to isolate the supernatant. For quantification of protein concentration, 3 ul of lysate was added to 300 ul of Precision Red (Cytoskeleton, Inc. ADV02-A) and absorbance (600 nm) was read on a plate reader and the concentration was calculated by: (Abs^sample – Abs^background) x 12.5. For Western blots, 10 μg of protein was resuspended in 2X Laemmli buffer and denatured at 100 C for 5 min. Samples were loaded and run on a 4–12% pre-cast Bis-Tris gel (Thermo NP0322BOX) and transferred overnight onto Nitrocellulose membrane (Thermo 88018). Membranes were blocked in 5% milk and primary antibodies were incubated overnight at 4 C. Blots were visualized using ECL (Perkin Elmer NEL104001EA).

**Statistical analysis.** All reported measurements are from distinct samples. When comparing samples across treatment groups, samples were collected, processed, and analyzed in parallel. In the figure legends, "*N*" refers to an independent biological replicate (e.g. single organoid or single monolayer culture). "Organoid" refers to an individual, distinct organoid from 1 well of culture dish. "Batch" refers to a group of organoids that were differentiated in the same dish on the same day. See Life Sciences Reporting Summary for more details. Statistical tests and biological replicates for each experiment are listed in the figure legends and in Supplementary Table 2.

**Reporting Summary.** Further information on research design is available in the Nature Research Reporting Summary linked to this article.

## Data Availability

The data that support the findings of this study are available from the corresponding author upon reasonable request.

## References

67. Dimidschstein, J. et al. A viral strategy for targeting and manipulating interneurons across vertebrate species. *Nat. Neurosci.* **19**, 1743–1749 (2016).
68. Lancaster, M. A. & Knoblich, J. A. Generation of cerebral organoids from human pluripotent stem cells. *Nat. Protoc.* **9**, 2329–2340 (2014).
69. Buglino, J. A. & Resh, M. D. Hhat is a palmitoylacyltransferase with specificity for N-palmitoylation of Sonic Hedgehog. *J. Biol. Chem.* **283**, 22076–22088 (2008).
70. Berthiaume, L., Peseckis, S. M. & Resh, M. D. Synthesis and use of iodo-fatty acid analogs. *Methods Enzymol.* **250**, 454–466 (1995).
71. Alland, L., Peseckis, S. M., Atherton, R. E., Berthiaume, L. & Resh, M. D. Dual myristylation and palmitylation of Src family member p59fyn affects subcellular localization. *J. Biol. Chem.* **269**, 16701–16705 (1994).

Corresponding author(s): Lorenz Studer

# Reporting Summary

Nature Research wishes to improve the reproducibility of the work that we publish. This form provides structure for consistency and transparency in reporting. For further information on Nature Research policies, see Authors & Referees and the Editorial Policy Checklist.

## Statistical parameters

When statistical analyses are reported, confirm that the following items are present in the relevant location (e.g. figure legend, table legend, main text, or Methods section).

| n/a | Confirmed | |
|---|---|---|
| ☐ | ☒ | The exact sample size ($n$) for each experimental group/condition, given as a discrete number and unit of measurement |
| ☐ | ☒ | An indication of whether measurements were taken from distinct samples or whether the same sample was measured repeatedly |
| ☐ | ☒ | The statistical test(s) used AND whether they are one- or two-sided<br>*Only common tests should be described solely by name; describe more complex techniques in the Methods section.* |
| ☒ | ☐ | A description of all covariates tested |
| ☐ | ☒ | A description of any assumptions or corrections, such as tests of normality and adjustment for multiple comparisons |
| ☐ | ☒ | A full description of the statistics including central tendency (e.g. means) or other basic estimates (e.g. regression coefficient) AND variation (e.g. standard deviation) or associated estimates of uncertainty (e.g. confidence intervals) |
| ☐ | ☒ | For null hypothesis testing, the test statistic (e.g. $F$, $t$, $r$) with confidence intervals, effect sizes, degrees of freedom and $P$ value noted<br>*Give P values as exact values whenever suitable.* |
| ☒ | ☐ | For Bayesian analysis, information on the choice of priors and Markov chain Monte Carlo settings |
| ☒ | ☐ | For hierarchical and complex designs, identification of the appropriate level for tests and full reporting of outcomes |
| ☒ | ☐ | Estimates of effect sizes (e.g. Cohen's $d$, Pearson's $r$), indicating how they were calculated |
| ☐ | ☒ | Clearly defined error bars<br>*State explicitly what error bars represent (e.g. SD, SE, CI)* |

*Our web collection on statistics for biologists may be useful.*

## Software and code

Policy information about availability of computer code

| | |
|---|---|
| Data collection | Zeiss Zen 2.3 Image Software and Olympus CellSens 1.15 were used for image acquisition. No custom software was used for data collection. |
| Data analysis | ImageJ v2.0 was used for image analysis. Adobe Photoshop v18 and Adobe Illustrator v21 were used for figure construction. |

For manuscripts utilizing custom algorithms or software that are central to the research but not yet described in published literature, software must be made available to editors/reviewers upon request. We strongly encourage code deposition in a community repository (e.g. GitHub). See the Nature Research guidelines for submitting code & software for further information.

## Data

Policy information about availability of data

All manuscripts must include a data availability statement. This statement should provide the following information, where applicable:
- Accession codes, unique identifiers, or web links for publicly available datasets
- A list of figures that have associated raw data
- A description of any restrictions on data availability

The data that support the findings of this study are available from the corresponding author upon reasonable request.

# Field-specific reporting

Please select the best fit for your research. If you are not sure, read the appropriate sections before making your selection.

☒ Life sciences          ☐ Behavioural & social sciences          ☐ Ecological, evolutionary & environmental sciences

For a reference copy of the document with all sections, see nature.com/authors/policies/ReportingSummary-flat.pdf

# Life sciences study design

All studies must disclose on these points even when the disclosure is negative.

| | |
|---|---|
| Sample size | Samples sizes for treatment experiments were not predetermined as there were no prior information on expected effect size and variability. At least 3 replicates were analyzed for each experiment in the main figures. |
| Data exclusions | Organoid samples were excluded from analysis based on pre-set quality control criteria, that were defined to ensure that samples had quantifiable forebrain neuroepithelial morphology.<br>1) Organoids failed to establish clear, budding neuroepithelium upon matrigel embedding as this indicates failed organization (Lancaster and Knoblich, 2014, Nat Protocol)<br>2) Organoids failed to induce FOXG1 expression (see Fig S2), as this indicates failed forebrain induction.<br>3) the SHH-organizer split into multiple clusters, as this could confound the analysis of patterning (see Fig S2). |
| Replication | Experimental findings were reproducible for samples that passed quality control criteria (see data exclusion). To ensure reproducibility organoids were analyzed from at least 2 independent batches, except where noted in the figure legend. |
| Randomization | Samples were consecutively assigned to treatment groups (i.e. samples 1-4: Group 1; samples 5-8: Group 2; etc.) |
| Blinding | Experimenter was not blind to group allocation for image acquisition and analysis. Organoid topography was quantified using standardized intensity thresholds across comparative groups. |

# Reporting for specific materials, systems and methods

## Materials & experimental systems

| n/a | Involved in the study |
|---|---|
| ☐ | ☒ Unique biological materials |
| ☐ | ☒ Antibodies |
| ☐ | ☒ Eukaryotic cell lines |
| ☒ | ☐ Palaeontology |
| ☒ | ☐ Animals and other organisms |
| ☒ | ☐ Human research participants |

## Methods

| n/a | Involved in the study |
|---|---|
| ☒ | ☐ ChIP-seq |
| ☒ | ☐ Flow cytometry |
| ☒ | ☐ MRI-based neuroimaging |

## Unique biological materials

Policy information about availability of materials

| Obtaining unique materials | Unique materials (e.g. iSHH cell line) are available from the authors upon request. |
|---|---|

## Antibodies

| Antibodies used | Antigen, Supplier, Catalog Number, Host Species, Clone Name (if applicable)<br>SHH, DSHB, 5E1, mouse, 5E1<br>SHH, Santa Cruz, 365112, mouse, E1<br>SHH, Santa Cruz, 9024, Rabbit<br>PAX6, Biolegend, 901301, rabbit, Polyclonal<br>PAX6, BD Biosciences, 561462, mouse, O18-561462<br>NKX2.1, Abcam, ab76013, rabbit, EP1584Y<br>NKX2.1, Thermo, MA5-13691, mouse, 8G7G3/1<br>NKX2.2, DSHB, 74.5A5, mouse, 74.5A5<br>FOXG1, Clontech, M227, rabbit, polyclonal<br>OTX2, Neuromics, GT15095, goat polyclonal |
|---|---|

GSH2, Millipore, ABN162, rabbit polyclonal
Acetylated Tubulin, Abcam, ab179484, rabbit, EPR16772
ZO-1, BD Biosciences, 610966, mouse, 1/ZO-1
Actin, BD Biosciences, 612657, mouse, C4
TCF7L2, Cell Signaling Tech, 2569, rabbit, C48H11

| Validation | Antibody validation statement by manufacturer and/or citation |
|---|---|
| | SHH, DSHB, 5E1: human reactivity validated by manufacturer, also (Ericson et al. (1996) Cell) |
| | SHH, Santa Cruz, 365112: human reactivity validated by manufacturer |
| | SHH, Santa Cruz, 9024: human reactivity validated by manufacturer |
| | PAX6, Biolegend, 901301: human reactivity validated by manufacturer, also (Tang et al. (2012) Development) |
| | PAX6, BD Biosciences, 561462: human reactivity validated by manufacturer, also (Chambers et al. (2009) Nat Biotech) |
| | NKX2.1, Abcam, ab76013: human reactivity validated by manufacturer, also (Radonijic et al. (2014) Front Neuroanat) |
| | NKX2.1, Thermo, MA5-13691: human reactivity validated by manufacturer, also (Di Palma et al. (2003) JBC) |
| | NKX2.2, DSHB, 74.5A5,: human reactivity validated by manufacturer, also (Ericson et al. (1997) Cell) |
| | FOXG1, Clontech, M227: human reactivity validated (Kadoshima et al. (2013) PNAS) |
| | OTX2, Neuromics, GT15095: human reactivity validated by manufacturer, also (Sonntag et al. (2007) Stem Cells). |
| | GSH2, Millipore, ABN162: mouse reactivity validated by manufacturer, also (Lancaster et al. (2017) Nat Biotech) |
| | Acetylated Tubulin, Abcam, ab179484: EPR16772, human reactivity validated by manufacturer |
| | ZO-1, BD Biosciences, 610966: human reactivity validated by manufacturer |
| | Actin, BD Biosciences, 612657: human reactivity validated by manufacturer |
| | TCF7L2, Cell Signaling Tech, 2569: human reactivity validated by manufacturer, also (Shiraishi et al. (2017) Development) |

# Eukaryotic cell lines

Policy information about cell lines

| Cell line source(s) | H9 - WiCell |
|---|---|
| | MEL1 - Stem Cells Ltd |
| | HUES6 / HUES8 - Harvard University |
| | LHX6-Citrine - University of Pennsylvania (S. Anderson) |
| | J1 / 348 iPSC - MSKCC |

| Authentication | STR Analysis was used to authenticate H9 and MEL1 lines |
|---|---|

| Mycoplasma contamination | Cell lines are regularly tested and were always negative for mycoplasma |
|---|---|

| Commonly misidentified lines (See ICLAC register) | No commonly misidentified lines used |
|---|---|